Supporting Information

Investigation on fluorescein derivatives with thermally activated delayed

fluorescence and their applications in imaging

Zhaoye Lv,[a] Jun Hou,[a] Junjie Yao,[a] Ye Yuan,[a] Yulan Qian,[a] Junyang Zhu,[a] Hongjuan

Zhao,[a] Xiaoqing Xiong[*ab] and Chengqi Jiao[**c]

[a] Key Lab of Textile Cleaning, Dalian Polytechnic University, #1 Qinggongyuan,

Dalian, 116034, P. R. China.

[b] State Key Laboratory of Fine Chemicals, Dalian University of Technology, #2

Linggong Road, Dalian, 116024, P. R. China.

[c] School of Chemistry and Chemical Engineering, Liaoning Normal University, 850

Huanghe Road, Dalian 116029, P.R. China.

Tel: +86-041186332096

E-mail: xiongxq@dlpu.edu.cn; jiaocq@lnnu.edu.cn

(This supporting information includes two schemes, twenty-six figures and ten tables

in thirty-three pages.)

General information

^{1}H-NMR and ^{13}C-NMR spectra were recorded on a VARIAN INOVA-400 spectrometer with chemical shifts reported as ppm (in DMSO or methanol, TMS as internal standard). The following abbreviations are used to indicate the multiplicities: s, singlet; d, doublet; t, triplet; q, quartet; m, multiplet; br, broad. Mass spectrometric data were obtained on a Q-TOF Micro mass spectrometry. Absorption spectra were measured on a Perkine Elmer Lambda35 UV-Vis spectrophotometer. Steady-state fluorescence was measured by a Varian Cary Eclipse fluorescence spectrophotometer (Serial No.: FL1109M018). Time-resolved luminescence spectra were obtained using a Perkin-Elmer LS 50B luminescence spectrometer with the following settings: total decay time, 5 ms; delay time, 0.1 ms; gate time, 1.0 ms; cycle time, 20 ms; excitation and emission slits, 15 nm. Nanosecond time-resolved transient absorption spectra were obtained using an LP920 laser flash photolysis spectrometer (Edinburgh Instruments, UK). Nanosecond fluorescence lifetimes were measured using the TCSPC technique on a F900 system with laser excitation at 476.20 nm, and microsecond fluorescence lifetimes were measured by nanosecond pulsed OPO laser synchronized with spectrofluorometer. For the temperature-dependent experiment, the sample was placed in an Optistat DN-V liquid nitrogen cryostat (Oxford, UK) with temperatures controlled between 77 and 300 K. The direct detection technique was applied to measure microsecond lifetimes using a photomultiplier tube (PMT, R928).

Cell culture and staining

MCF-7 cell lines were cultured in DEME (Invitrogen) supplemented with 10%

FCS (Invitrogen). Then the pretreated MCF-7 cells were stained with **DCF-MPYA** (20 μM) and **FL** (20 μM) for 120 min at ambient temperature and then imaged with confocal fluorescence microscopy or time-resolved fluorescence microscopy. And a total of 40 μL BSA (10 mM) was added into the system and incubated at 37°C in 5% CO_2 for 2 h. Cells were rinsed by clean PBS three times before imaging. For each dye's test, the fluorescent imaging pictures were obtained with an almostly equal parameter for control.

Cell imaging measurements were obtained with spectral confocal microscopes (Olympus, FV1000). The time-resolved luminescence imaging measurements were carried out on a laboratory-use luminescence microscope. The microscope, equipped with a 30 W xenon flash-lamp (Pulse 300, Photonic Research Systems Ltd.), UV-2A filters (Nikon, excitation filter, 510–560 nm; dichroic mirror, 400 nm; emission filter, > 420 nm). And a time-resolved digital black-and- white CCD camera system (Photonic Research Systems Ltd.) was used for the time-resolved luminescence imaging measurement with the conditions of delaytime, 15 μs; gatetime, 100 ms; lamp-pulse width, 6 ms; and exposure time, 300 s. The time-resolved luminescence images are shown in pseudo-color treated by Simple PCI software.

MTT assay for the cell cytotoxicity

This involves the reduction of MTT (3-(4, 5-dimethylthiazol-2-yl)-2, 5-diphenyltetrazolium bromide) tetrazolium to MTT formazan pigment by the metabolic activity of living cells. COS-7 cells were seeded at a density of $1\sim10^5$ cells/mL in a 96-well plate. After 24 h of cell attachment, cells were treated with

DCF-MPYA and **FL** at experimental concentration (20 μM) from 0 h to 10 h. After incubation for 2 h, 4 h, 6 h, 8 h and 10 h, the medium was removed and cells were washed with PBS twice. MTT tetrazolium solution (100 mL of 0.5 mg/mL in PBS) was added to each well, and the cells were further incubated at 37°C for 4 h in a 5% CO_2 humidified atmosphere. Excess MTT tetrazolium solution was then carefully removed and the colored formazan was dissolved in 100 mL dimethyl sulfoxide (DMSO). The plate was shaken for 10 min and the absorbance was measured at 600 nm using a microplate reader.

Computational Method

Conformational search for different dyes in its neutral and anionic forms were preformed using the conformer-rotamer ensemble sampling (CREST) algorithm[1] that relies on the semi-empirical tight-binding based quantum chemistry method GFN2-xTB level[2] of XTB code[3] (version 6.1) in GBSA dimethyl sulfoxide solvent. The default settings and thresholds for the MTD-GC(RMSD)/GFN2-xTB simulation were used, in which an extensive root mean square deviation (RMSD) based meta-dynamics sampling (MTD)is performed with an extra genetic z matrix crossing (GC) step at the end[4].

All quantum mechanical calculations were used Gaussian 09 program software[5]. Geometry optimizations were performed with empirical dispersion corrected PBE0[6] functional (D3BJ damping[7]) and the 6-31G(d) basis set. Frequency analyses were calculated at the same level to confirm the nature of the stationary points as equilibrium structure with all real frequencies. All the thermodynamic quantities were

computed in the GoodVibes code[8] with quasi-harmonic corrections.[9] Higher level single-point energy calculations were performed at the PBE0-D3BJ/6-311++G(d, p) level with IEF-PCM model[10] with dimethyl sulfoxide as a solvent. The relative free energies reported in the conformational search were computed at PBE0-D3BJ/6-311++G(d, p)(SMD, DMSO)//PBE0-D3BJ/6-31+G(d) level. CYLview was used for molecular visualizations.[11] DFT and linear-response TD-DFT in combination with PBE0-D3BJ functional with 6-31G(d) basis set were employed to calculate the ground (S_0) and excited state (S_1) of the target molecules with lowest free energy. All calculations were conducted using the IEF-PCM model with dimethyl sulfoxide as a solvent. Electron excitation energy and emission energy were calculated in the assumed nonequilibrium and equilibrium solvation, respectively.
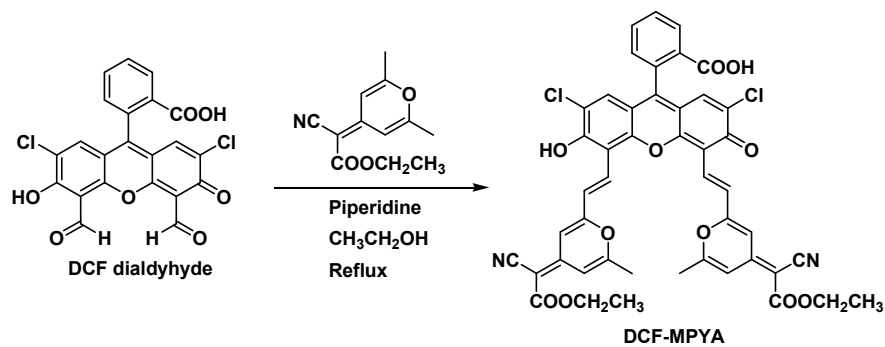
Scheme S1 Synthetic routines of the dye **DCF-MPYA**
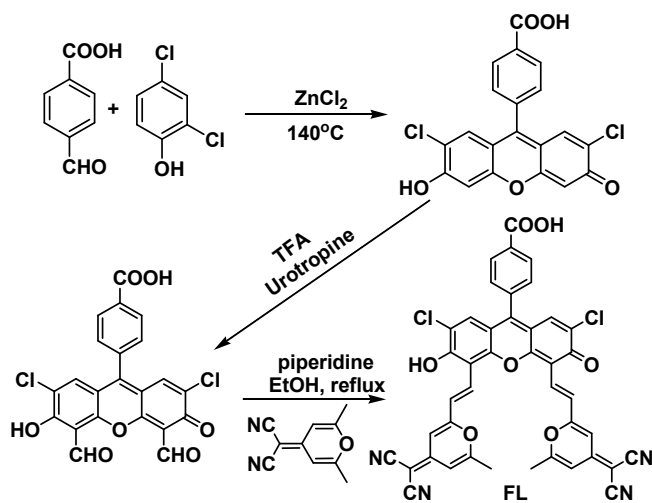
Scheme S2 Synthetic routines of the dye **FL**.
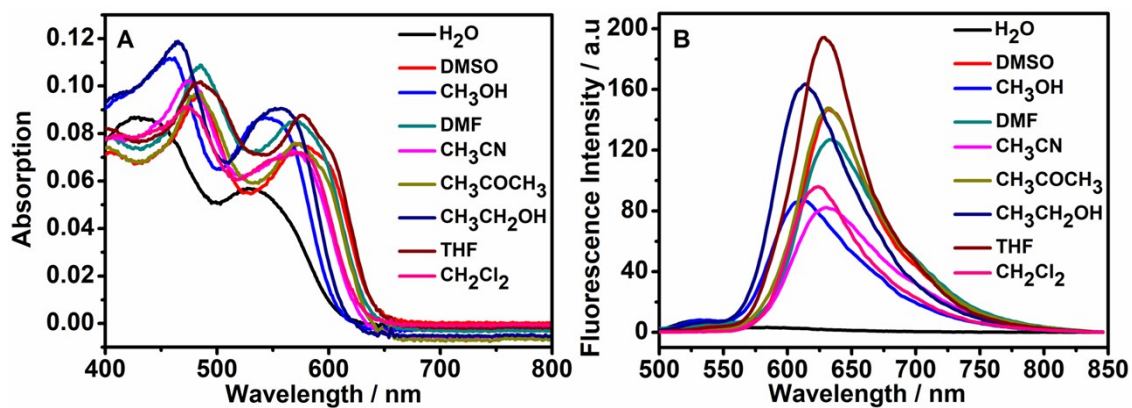
Fig. S1 (A) UV spectra of **DCF-MPYA** (2.0 μM) in different solvents. (B) fluorescent spectra of **DCF-MPYA** (2.0 μM) in different solvents.
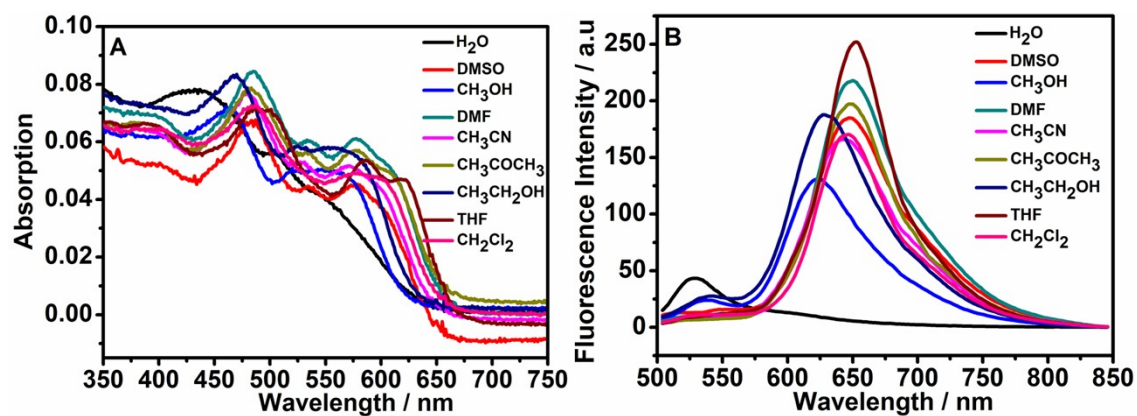
Fig. S2 (A) UV spectra of **FL** (2.0 μM) in different solvents. (B) fluorescent spectra of **FL** (2.0 μM) in different solvents.

Tab. S1 Photophysical properties of **DCF-MPYA** in different solvents

Solvents	λ_{ab1}[a]	λ_{ab2}[a]	λ_{em1}[a]	λ_{em2}[a]	$\varepsilon(\times10^5)$[b]	$\varepsilon(\times10^5)$[b]	Φ[c]	Stokes shift (nm)
H_2O	430	527	525	--	0.43	0.28	0.013	95
DMSO	483	573	--	632	0.48	0.38	0.24	149
CH_3OH	462	546	531	611	0.56	0.43	0.14	149
DMF	485	570	540	634	0.54	0.43	0.23	149
CH_3CN	474	568	540	631	0.51	0.36	0.14	157
CH_3COCH_3	485	569	--	632	0.48	0.38	0.23	147
CH_3CH_2OH	465	557	533	616	0.56	0.45	0.25	151
THF	485	576	--	629	0.51	0.44	0.30	144
CH_2Cl_2	475	575	489	624	0.46	0.36	0.13	149

[a]nm; [b]mol^{-1}cm^{-1}L; [c]Rhodamine B was used as a standard (Φ=0.69 in EtOH)[13].

Tab. S2 Photophysical properties of **FL** in different solvents

Solvents	λ_{ab1}[a]	λ_{ab2}[a]	λ_{em1}[a]	λ_{em2}[a]	$\varepsilon(\times10^5)$[b]	$\varepsilon(\times10^5)$[b]	Φ[c]	Stokes shift (nm)
H_2O	446	542	525	--	0.42	0.27	0.014	79
DMSO	485	571	--	644	0.32	0.25	0.25	159
CH_3OH	462	547	529	623	0.37	0.28	0.094	161
DMF	485	564	--	636	0.34	0.28	0.28	151
CH_3CN	473	570	--	644	0.35	0.22	0.096	171
CH_3COCH_3	479	565	--	644	0.36	0.26	0.20	176
CH_3CH_2OH	468	557	532	626	0.45	0.32	0.17	158
THF	486	574	--	645	0.37	0.30	0.33	159
CH_2Cl_2	472	568	--	636	0.32	0.25	0.21	164

[a]nm; [b]mol^{-1}cm^{-1}L; [c]Rhodamine B was used as a standard (Φ=0.69 in EtOH)[13].
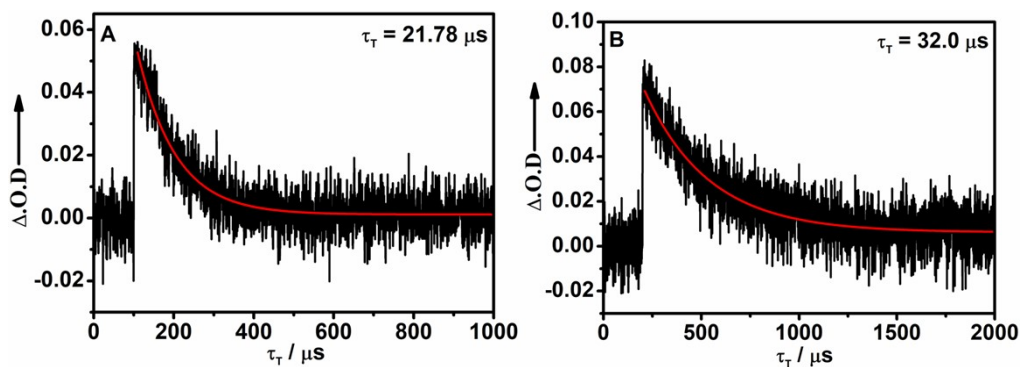
Fig. S3 (A) Decay trace of **DCF-MPYA** (2.0×10^{-5} M in ethanol) at 465 nm after pulsed laser excitation ($\lambda_{ex} = 355$ nm) under N_2 atmosphere. (B) Decay trace of **FL** (2.0×10^{-5} M in ethanol) at 465 nm after pulsed laser excitation ($\lambda_{ex} = 355$ nm) under N_2 atmosphere.
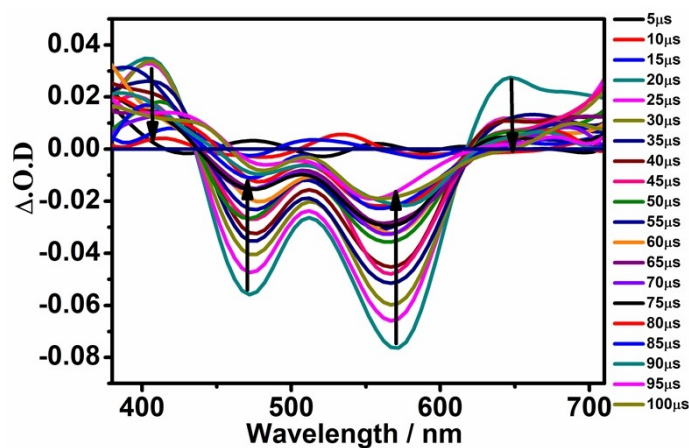
Fig. S4 Nanosecond time-resolved transient difference absorption spectra of **FL** (2.0×10^{-5} M in deaerated ethanol) with different delay time, excitation wavelength at 532 nm.
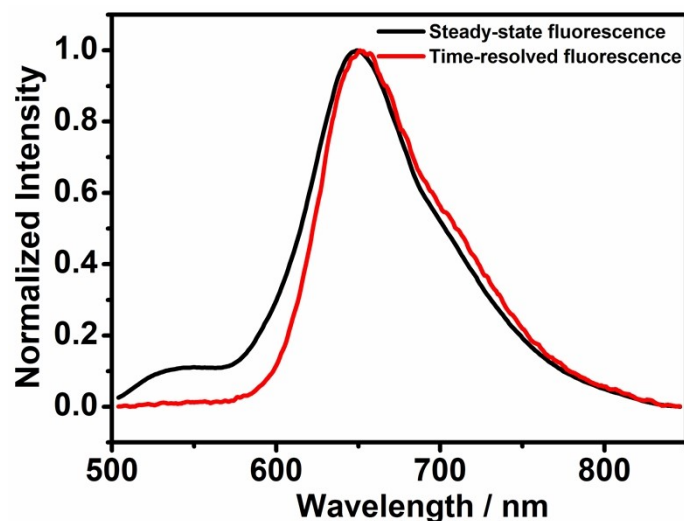
Fig. S5 Normalized emission spectra for **FL** (10.0 μM in deaerated CH_3CN). Black line: Steady-state fluorescence spectrum under air atmosphere (delay time, 0 s). Red line: time-resolved fluorescence spectrum under N_2 atmosphere. All the delayed detection was carried out in phosphorescence mode (total decay time, 5 ms; delay time, 0.1 ms; gate time, 1.0 ms), and the excitation wavelength was 465 nm.
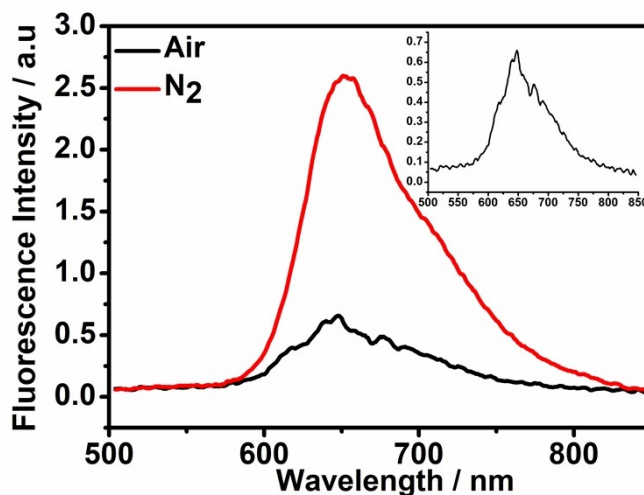
Fig. S6 Time-resolved fluorescence spectra for **FL** (10.0 μM in CH_3CN). Black line: time-resolved fluorescence spectrum under Air atmosphere. Red line: time-resolved fluorescence spectrum under N_2 atmosphere. All the delayed detection was carried out in phosphorescence mode (total decay time, 5 ms; delay time, 0.1 ms; gate time, 1.0 ms), and the excitation wavelength was 465 nm.
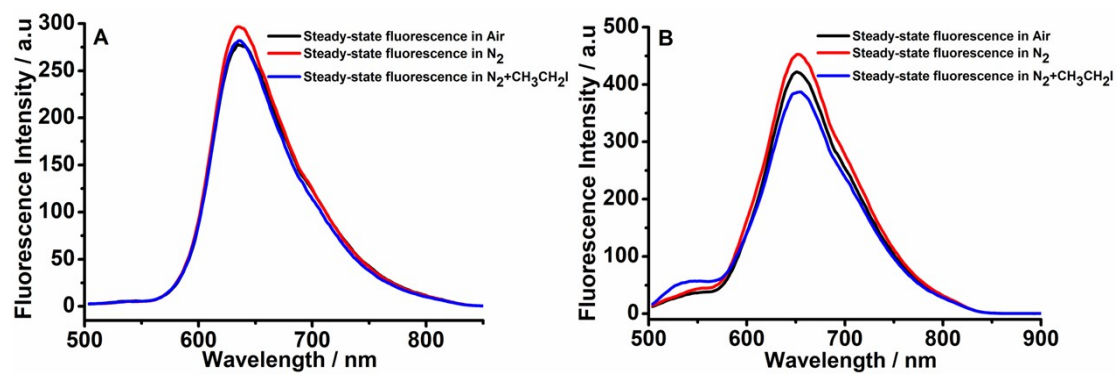
Fig. S7 Prompt emission spectra for **DCF-MPYA** (A, 10.0 μM in CH_3CN) and **FL** (B, 10.0 μM in CH_3CN). Black line: steady-state fluorescence spectrum under Air atmosphere; red line: steady-state fluorescence spectrum under N_2 atmosphere; blue line: steady-state fluorescence spectrum after the addition of CH_3CH_2I under N_2 atmosphere. All the detection was carried out in fluorescence mode and the excitation wavelength was 465 nm.
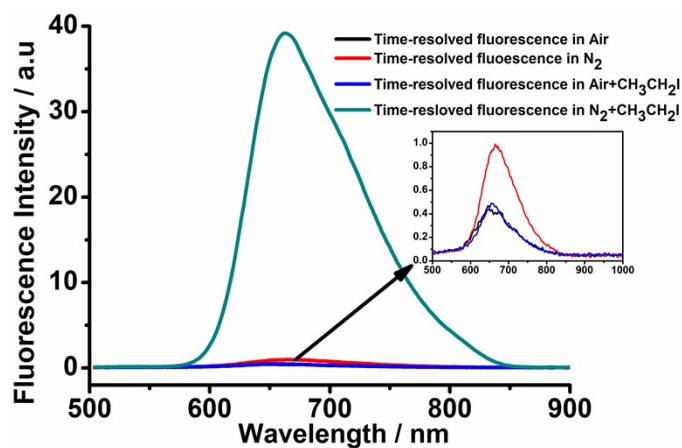
Fig. S8 Time-resolved fluorescence spectra for **FL** (10.0 μM in CH_3CN). Black line: time-resolved fluorescence spectrum under Air atmosphere; red line: time-resolved fluorescence spectrum under N_2 atmosphere; blue line: time-resolved fluorescence spectrum after the addition of CH_3CH_2I under Air atmosphere; dark cyan line: time-resolved fluorescence spectrum after the addition of CH_3CH_2I under N_2 atmosphere. Inset is the enlarged view of spectra with low fluorescence intensity. All the delayed detection was carried out in phosphorescence mode (total decay time, 5 ms; delay time, 0.1 ms; gate time, 1.0 ms), and the excitation wavelength was 465 nm.
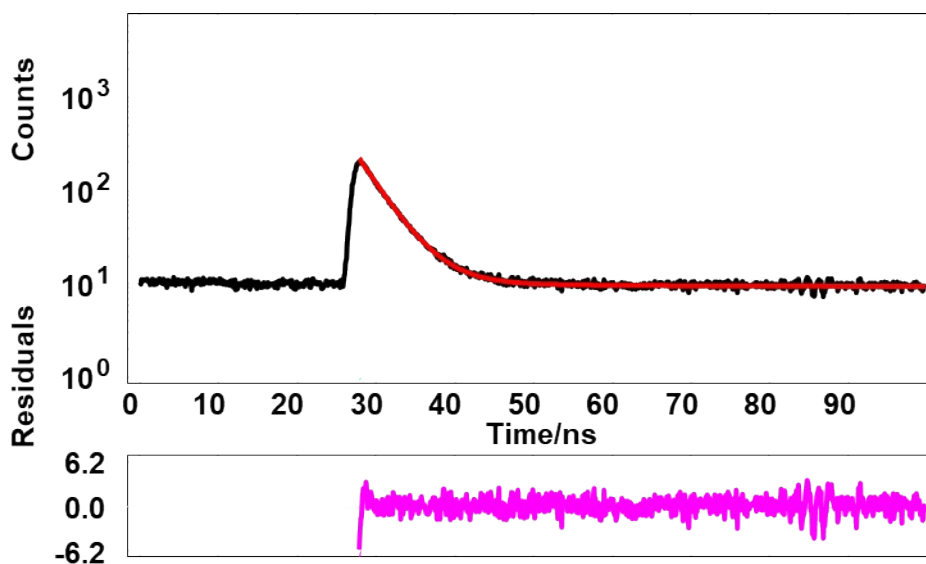
Fig. S9 Prompt decay of **DCF-MPYA** (2.0×10^{-5} mol/L) in CH_3CN at room temperature, excitation wavelength was 476.20 nm, monitored emission wavelength was 645 nm.
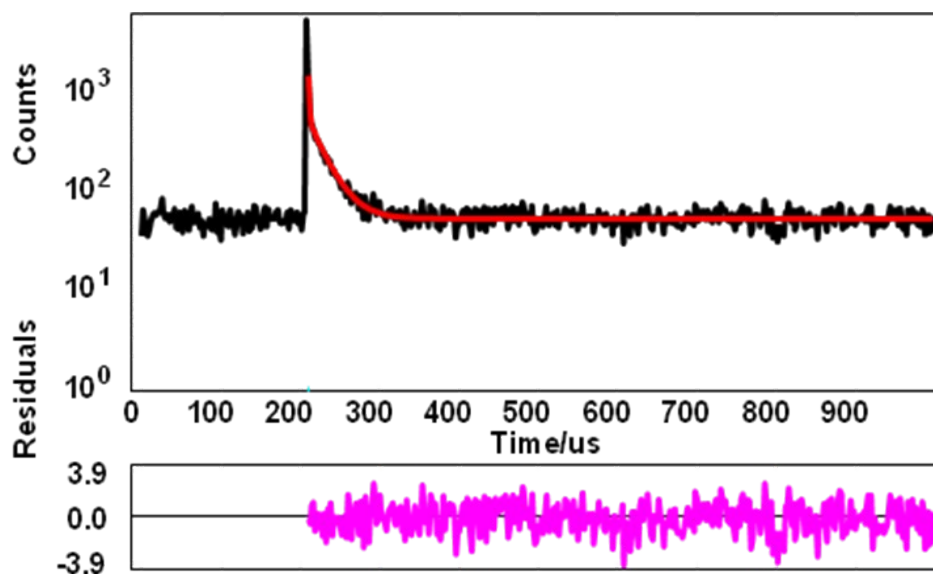
Fig. S10 Emission decay of **DCF-MPYA** (2.0×10^{-5} mol/L) in CH_3CN at room temperature, curves show the profiles after deoxygenating ($\tau = 13.16$ μs). Monitored emission wavelength was 645 nm.
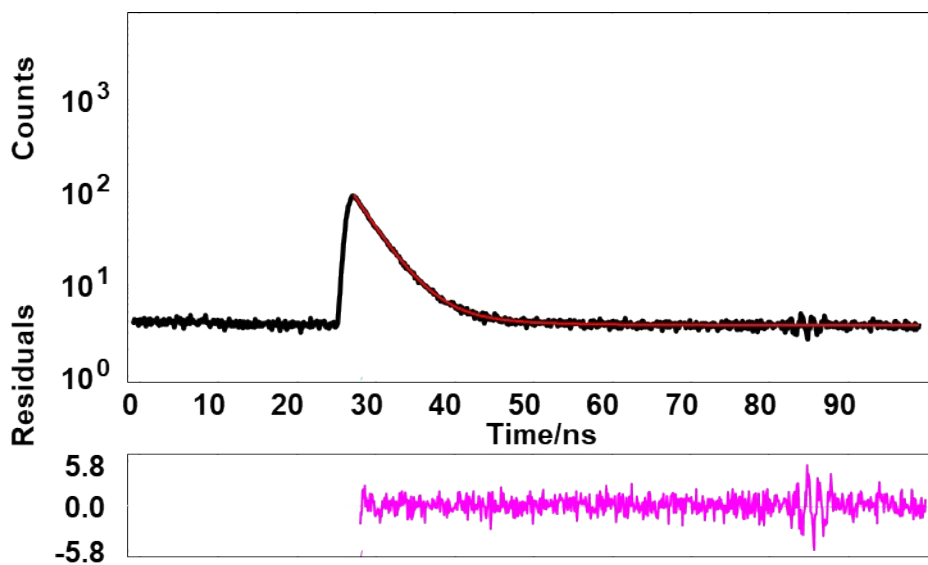
Fig. S11 Prompt decay of **FL** (2.0×10^{-5} mol/L) in CH_3CN at room temperature, excitation wavelength was 476.20 nm, monitored emission wavelength was 651 nm.
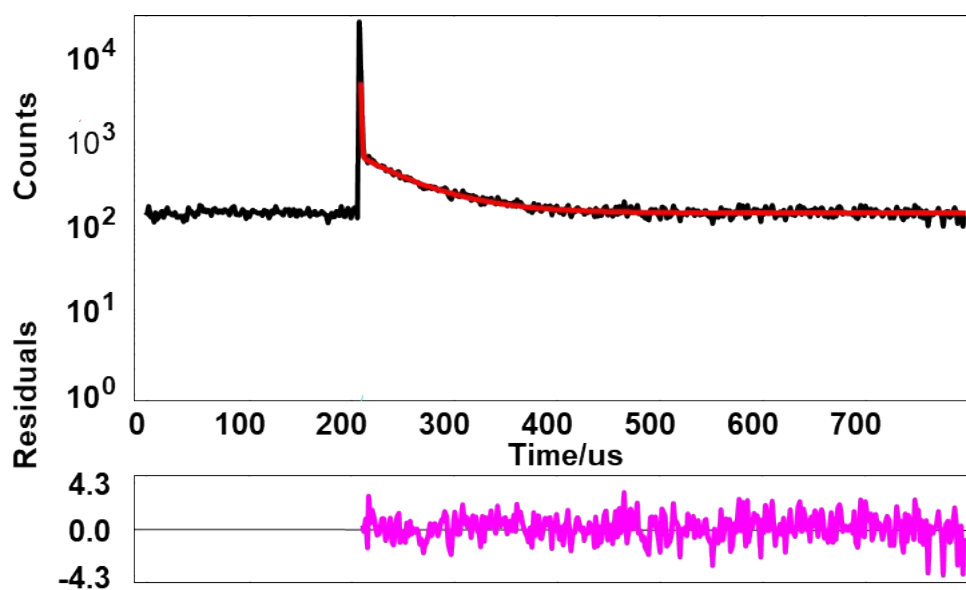
Fig. S12 Emission decay of **FL** (2.0×10^{-5} mol/L) in CH_3CN at room temperature, curves show the profiles after deoxygenating ($\tau = 23.72$ μs), monitored emission wavelength was 651 nm.

Tab. S3 Fluorescent lifetime compositions of prompt components for **DCF-MPYA** in deaerated CH_3CN. Excitation with a 476.20 nm picosecond laser, the decay of the emission was monitored at 645 nm.

Monitoring wavelength (nm)	τ_1 (ns)[a]	n_1%[b]	τ_2 (ns)[a]	n_2%[b]	τ_p (ns) [c]
634 (deaerated)	3.31	96.00	25.61	0.04	4.20

[a]Obtained from the double-exponential fitting of transient decay curves on a 100 ns scale; [b]The contribution of each component to average lifetime; [c]The average fluorescence lifetime of prompt component.

Tab. S4 Fluorescent lifetime compositions of prompt components for **FL** in deaerated CH_3CN. Excitation with a 476.20 nm picosecond laser, the decay of the emission was monitored at 651 nm.

Monitoring wavelength (nm)	τ_1 (ns)[a]	n_1%[b]	τ_2 (ns)[a]	n_2%[b]	τ_p (ns) [c]
640 (deaerated)	3.21	93.85	10.67	6.15	3.67

[a]Obtained from the double-exponential fitting of transient decay curves on a 100 ns scale; [b]The contribution of each component to average lifetime; [c]The average fluorescence lifetime of prompt component.

Tab. S5 Luminescence lifetime compositions of **DCF-MPYA** (20.0 μM in CH₃OH/CH₃CH₂OH = 5/4 (v/v)) in different temperatures. Excited at 485 nm (nanosecond pulsed OPO laser synchronized with spectrofluorometer) and monitored at 634 nm.

Temperature	τ_1 (μs)[a]	n_1%[b]	τ_2 (μs)[a]	n_2%[b]	τ_d (μs) [c]
77 K	0.94	46.38	11.26	53.62	6.48
100 K	0.96	47.45	11.72	52.55	6.61
140 K	0.95	47.72	11.79	52.28	6.62
180 K	0.87	51.81	11.75	48.19	6.12
220 K	0.83	51.02	11.24	48.98	5.99
260 K	0.91	52.46	11.24	47.54	5.82
300 K	0.87	52.11	10.89	47.89	5.67

[a]Obtained from the double-exponential fitting of transient decay curves on an 800 μs scale; [b]The contribution of each component to average lifetime; [c]The average fluorescence lifetime of delayed component.

Tab. S6 Luminescence lifetime compositions of **FL** (20.0 μM in CH_3OH/CH_3CH_2OH = 5/4(v/v)) in different temperatures. Excited at 485 nm (nanosecond pulsed OPO laser synchronized with spectrofluorometer) and monitored at 640 nm.

Temperature	τ_1 (μs)[a]	n_1%[b]	τ_2 (μs)[a]	n_2%[b]	τ_d (μs) [c]
77 K	1.30	39.24	12.92	60.76	8.37
100 K	1.31	37.55	12.95	62.45	8.58
140 K	1.33	37.54	13.14	62.46	8.64
180 K	1.22	43.14	12.84	56.86	7.32
220 K	0.98	50.80	12.24	49.14	6.26
260 K	0.89	52.39	11.68	47.61	5.78
300 K	0.91	52.62	11.48	47.38	5.67

[a]Obtained from the double-exponential fitting of transient decay curves on an 800 μs scale; [b]The contribution of each component to average lifetime; [c]The average fluorescence lifetime of delayed component.
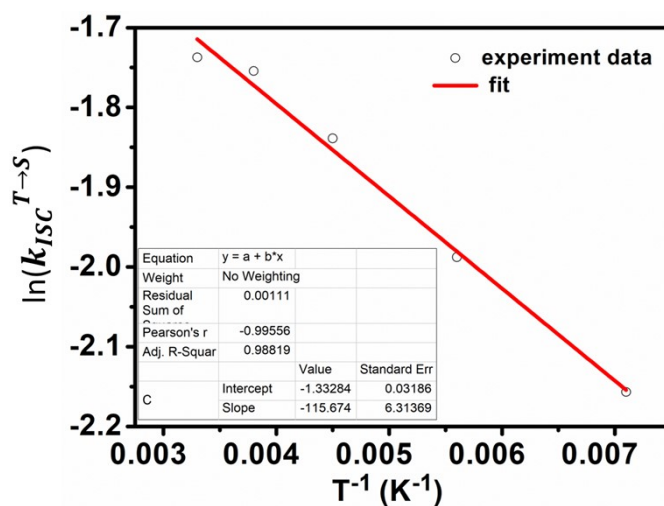
Fig. 13 Logarithm of the fluorescence decay rate vs the reciprocal of temperature for **FL**; red line represents the fitting curves that obtained on the basis of equation 1.

Conformer 1
0.0 kcal/mol (64.42%)

Conformer 2
0.4 kcal/mol (32.80%)

Conformer 3
2.1 kcal/mol (1.86%)

Conformer 4
2.9 kcal/mol (0.48%)

Conformer 5
3.3 kcal/mol (0.25%)

Conformer 6
3.5 kcal/mol (0.18%)

Conformer 7
5.1 kcal/mol (0.01%)

Conformer 8
5.6 kcal/mol (0.01%)
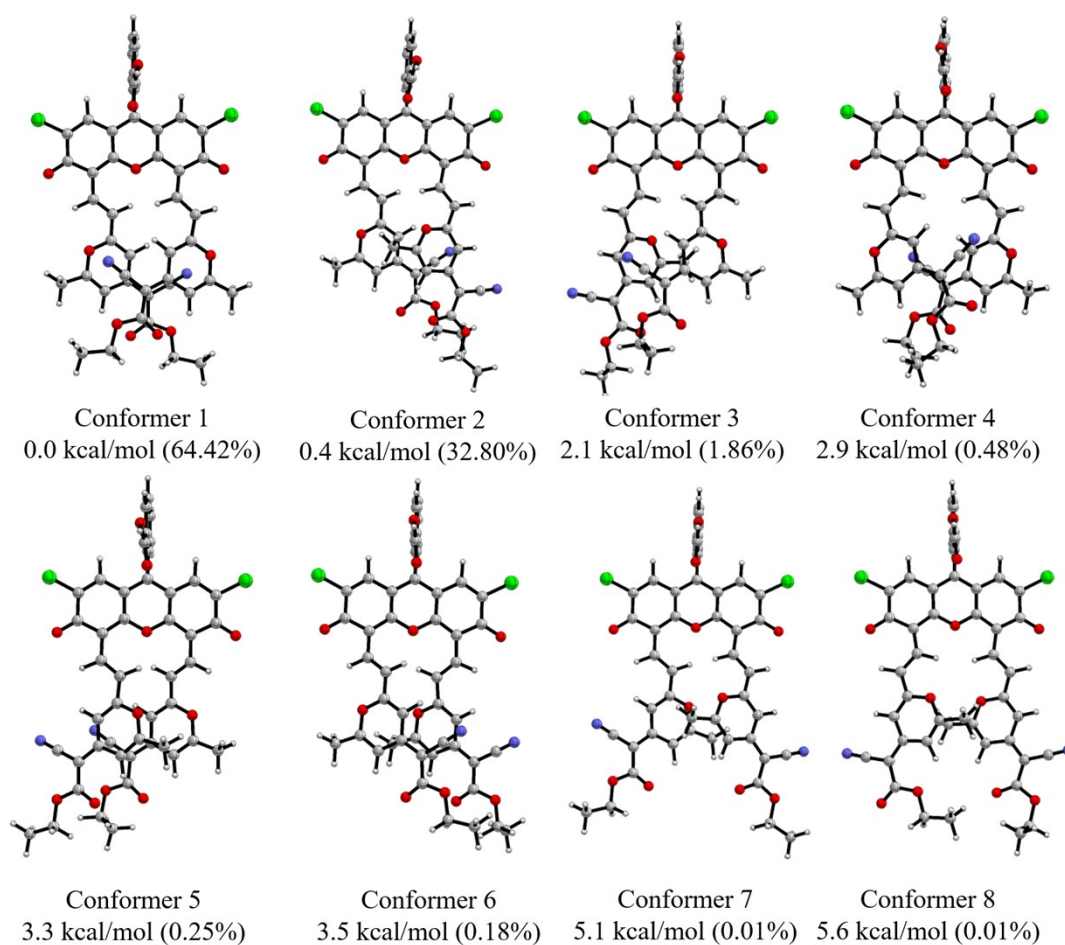
Fig. S14 Different conformers of **[DCF-MPYA-H]**⁻ with corresponding relative free energy (kcal/mol) and Boltzmann population (value in parentheses).

Conformer 1
0.0 kcal/mol (59.84%)

Conformer 2
0.3 kcal/mol (36.06%)

Conformer 3
1.8 kcal/mol (2.87%)

Conformer 4
2.6 kcal/mol (0.74%)

Conformer 5
3.2 kcal/mol (0.27%)

Conformer 6
3.4 kcal/mol (0.19%)

Conformer 7
4.8 kcal/mol (0.02%)

Conformer 8
5.1 kcal/mol (0.01%)
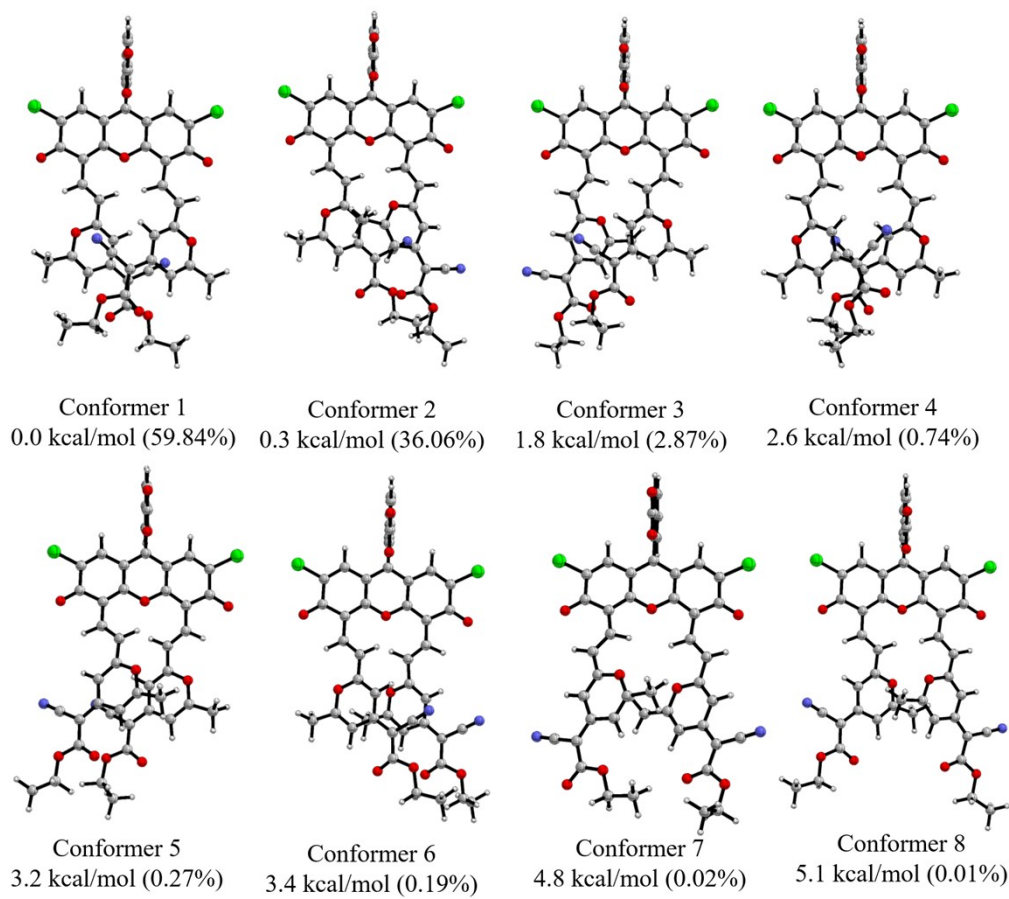
Fig. S15 Different conformers of **[DCF-MPYA-2H]$^{2-}$** with corresponding relative free energy (kcal/mol) and Boltzmann population (value in parentheses).

Conformer 1
0.0 kcal/mol (43.96%)

Conformer 2
0.1 kcal/mol (37.14%)

Conformer 3
0.9 kcal/mol (9.62%)

Conformer 4
1.0 kcal/mol (8.13%)

Conformer 5
2.7 kcal/mol (0.46%)

Conformer 6
2.8 kcal/mol (0.39%)

Conformer 7
3.1 kcal/mol (0.23%)

Conformer 8
3.9 kcal/mol (0.06%)
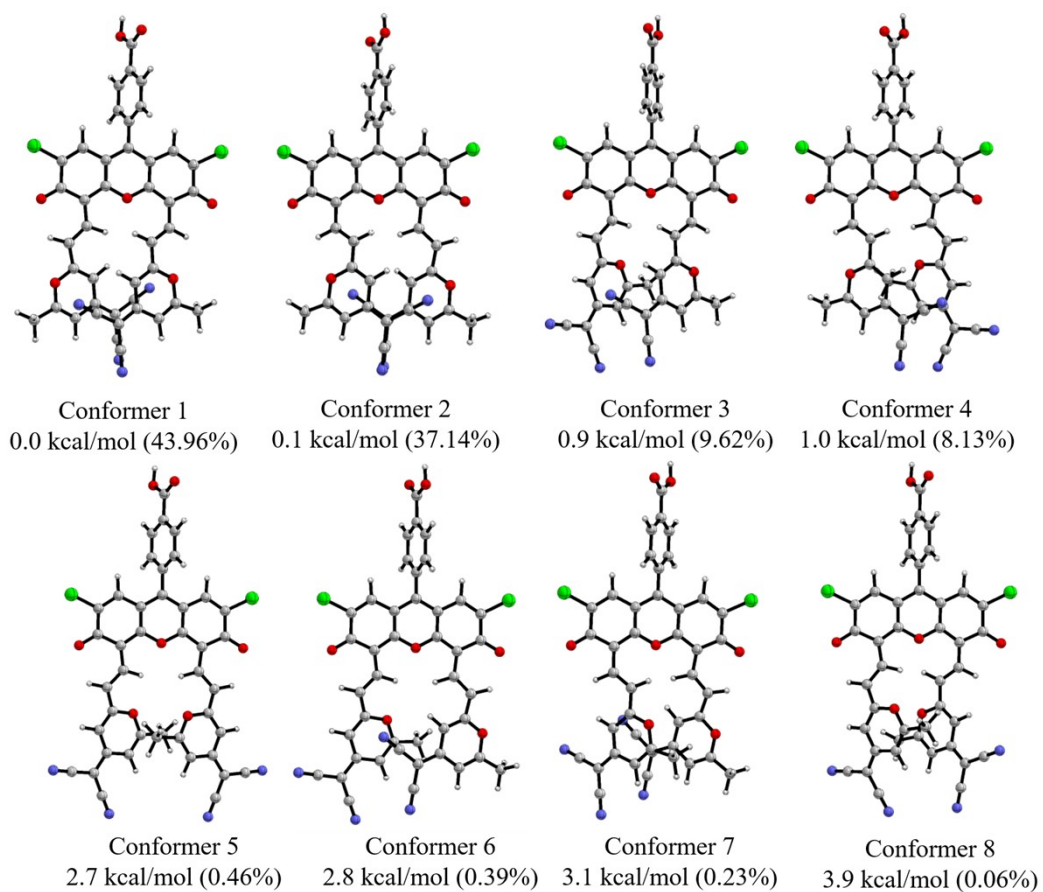
Fig. S16 Different conformers of **[FL-H]**⁻ with corresponding relative free energy

(kcal/mol) and Boltzmann population (value in parentheses).
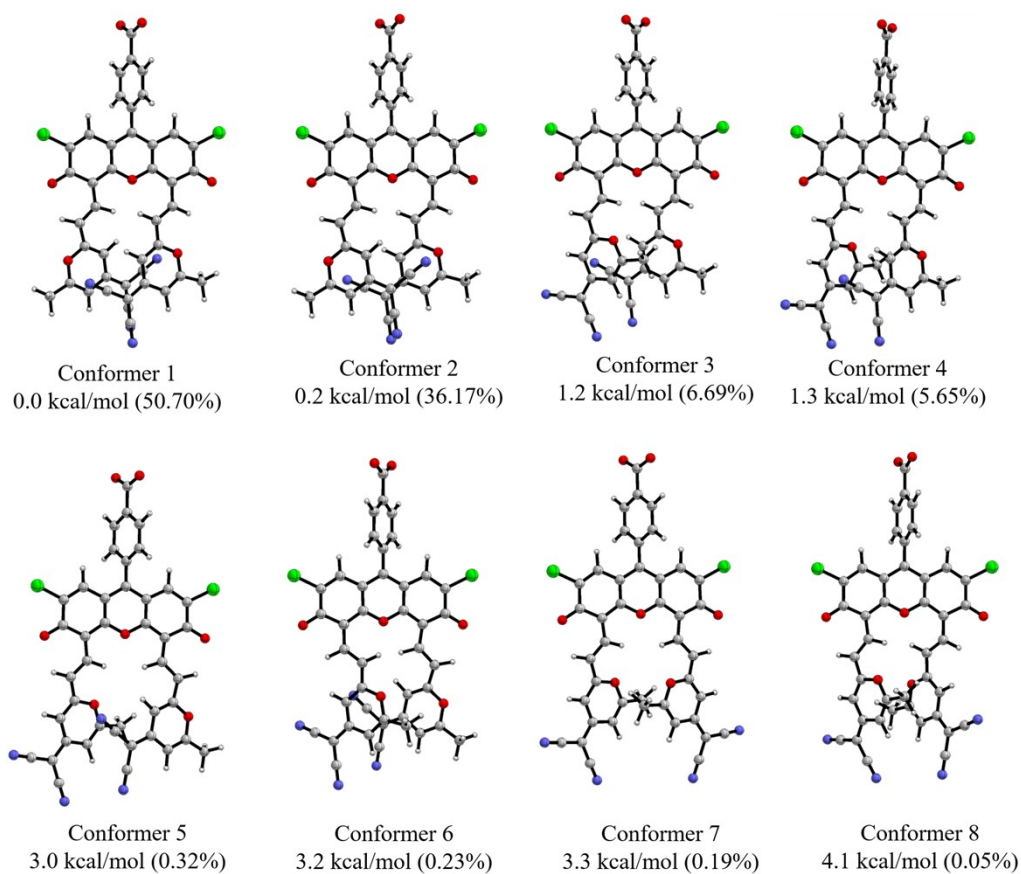
Fig. S17 Different conformers of **[FL-2H]$^{2-}$** with corresponding relative free energy (kcal/mol) and Boltzmann population (value in parentheses).
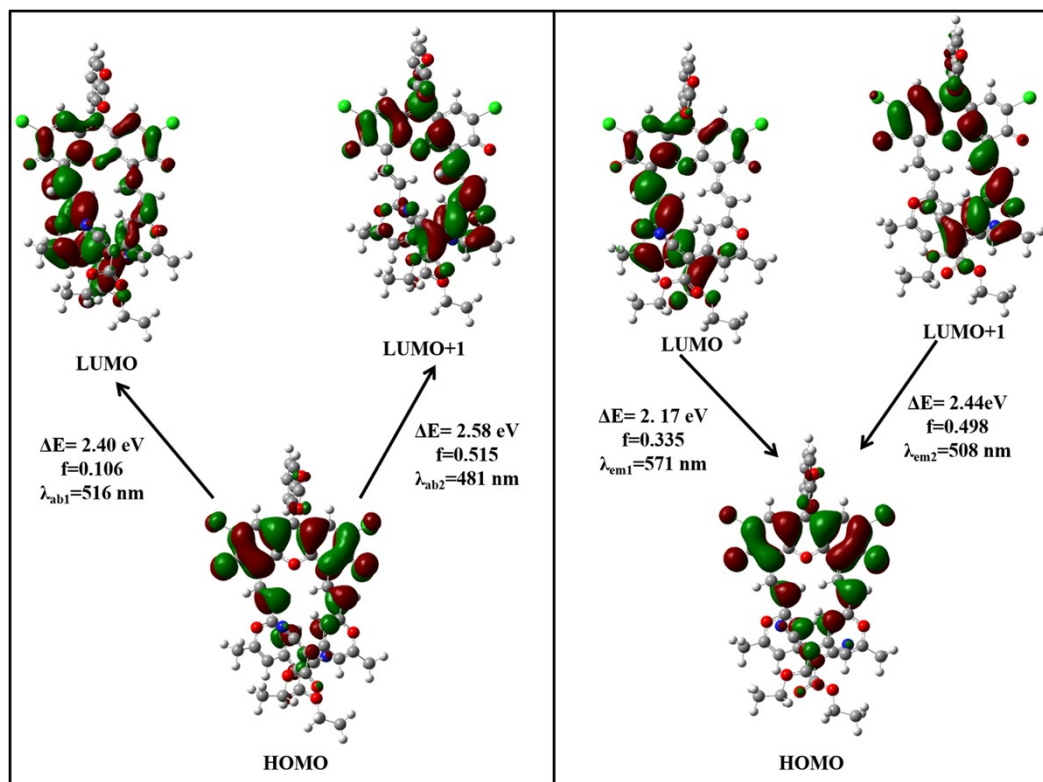
Fig. S18 Frontier molecular orbital plots of **[DCF-MPYA-2H]²⁻** in DMSO; they are involved in vertical excitation (UV–vis absorption) and emission.
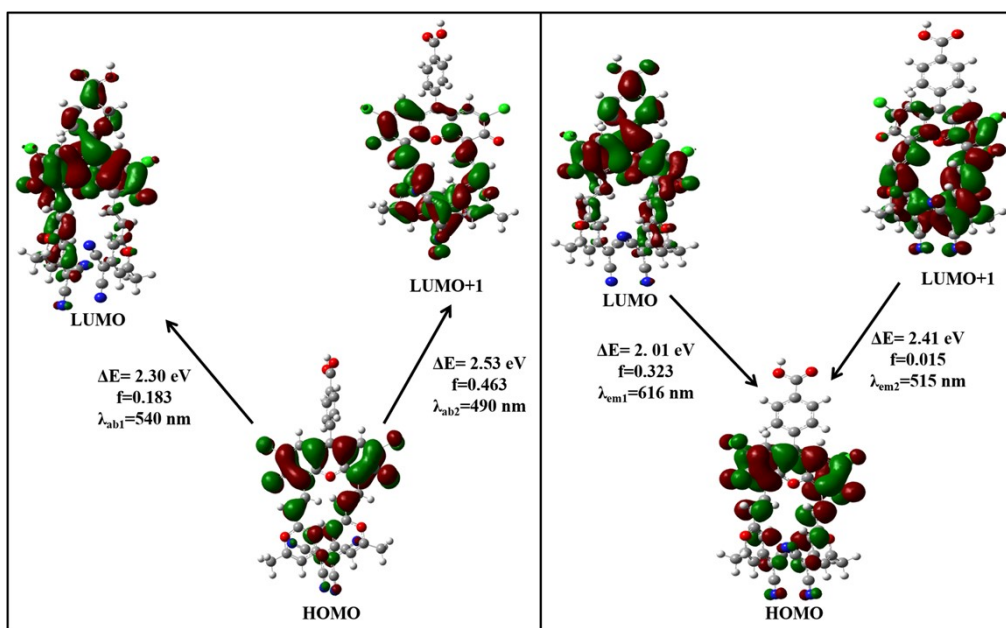
Fig. S19 Frontier molecular orbital plots of **[FL-H]⁻** in DMSO; they are involved in vertical excitation (UV–vis absorption) and emission.
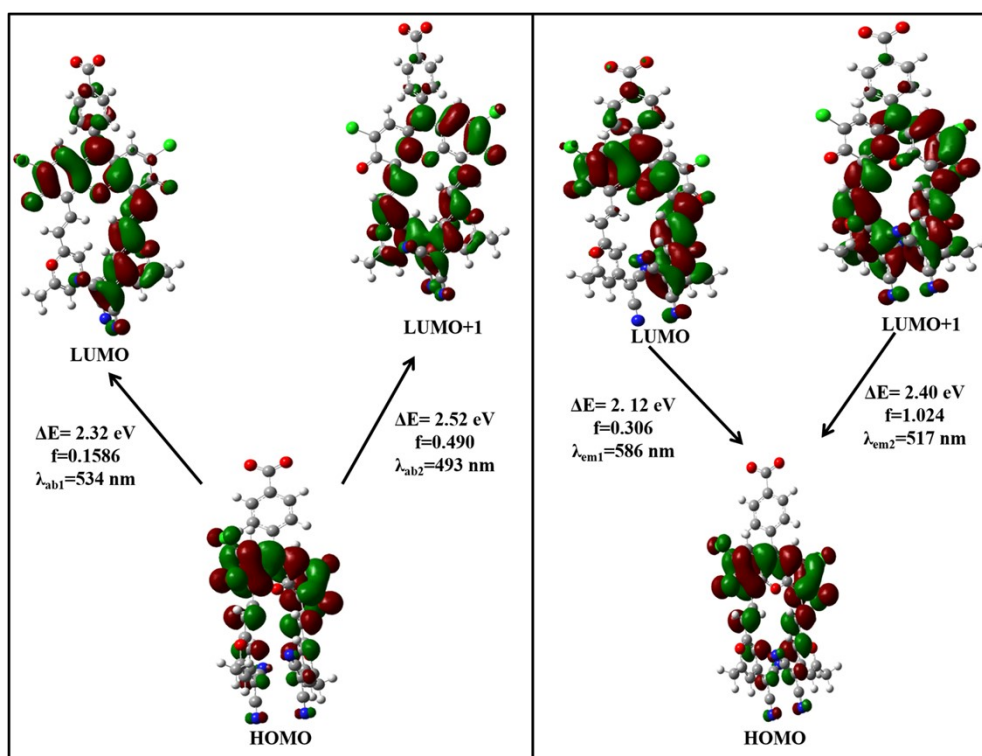
Fig. S20 Frontier molecular orbital plots of **[FL-2H]²⁻** in DMSO; they are involved in vertical excitation (UV–vis absorption) and emission.

Tab. S7 Calculated electronic transition data in terms of excitation energies (E/eV), absorption wavelengths (λ_{ab}/nm), oscillator Strengths (f_{ab}), and electronic compositions for **[DCF-MPYA-H]⁻** and **[FL-H]⁻** in DMSO.

Compound	Electronic transition[a]	Excitation energy (λ_{ab}/nm)	f [b]	Composition [c]	CI [d]
[DCF-MPYA-H]⁻	$S_0 \rightarrow S_1$	2.39 eV (519)	0.166	H→L	0.62
	$S_0 \rightarrow S_2$	2.63 eV (472)	0.502	H→L+1	0.68
[FL-H]⁻	$S_0 \rightarrow S_1$	2.30 eV (540)	0.183	H→L	0.64
	$S_0 \rightarrow S_2$	2.53 eV (490)	0.463	H→L+1	0.68

[a] Only selected excitation states were considered. The numbers in parentheses are the excitation energy in wavelength. [b] Oscillator strength. [c] H stands for HOMO and L stands for LUMO. Only the configurations are presented. [d] Coefficient of the wave function for excitations. The CI coefficients are in absolute values.

Tab. S8 Calculated electronic transition data in terms of excitation energies (E/eV), absorption wavelengths (λ_{ab}/nm), oscillator Strengths (f_{ab}), and electronic compositions for **[DCF-MPYA-2H]$^{2-}$** and **[FL-2H]$^{2-}$** in DMSO.

Compound	Electronic transition[a]	Excitation energy (λ_{ab}/nm)	f [b]	Composition [c]	CI [d]
[DCF-MPYA-2H]$^{2-}$	$S_0 \rightarrow S_1$	2.40 eV (534)	0.106	H→L	0.42
	$S_0 \rightarrow S_2$	2.58 eV (481)	0.515	H→L+1	-0.40
[FL-2H]$^{2-}$	$S_0 \rightarrow S_1$	2.32 eV (534)	0.1586	H→L	0.63
	$S_0 \rightarrow S_2$	2.52 eV (493)	0.490	H→L+1	0.65

[a] Only selected excitation states were considered. The numbers in parentheses are the excitation energy in wavelength. [b] Oscillator strength. [c] H stands for HOMO and L stands for LUMO. Only the configurations are presented. [d] Coefficient of the wave function for excitations. The CI coefficients are in absolute values.

Tab. S9 Calculated electronic transition data in terms of excitation energies (E/eV), emission wavelengths (λ_{em}/nm), oscillator strengths (f_{em}), and electronic compositions for **[DCF-MPYA-H]⁻** and **[FL-H]⁻** in DMSO.

Compound	Electronic transition[a]	Excitation energy (λ_{ab}/nm)	f[b]	Composition[c]	CI[d]
[DCF-MPYA-H]⁻	$S_1{\rightarrow}S_0$	2.07 eV (600)	0.317	H→L	-0.68
	$S_2{\rightarrow}S_0$	2.43 eV (509)	0.211	H-1→L	0.69
[FL-H]⁻	$S_1{\rightarrow}S_0$	2.01 eV (616)	0.323	H→L	0.68
	$S_2{\rightarrow}S_0$	2.41 eV (515)	0.015	H→L+1	0.30

[a] Only selected excitation states were considered. The numbers in parentheses are the excitation energy in wavelength. [b] Oscillator strength. [c] H stands for HOMO and L stands for LUMO. Only the configurations are presented. [d] Coefficient of the wave function for excitations. The CI coefficients are in absolute values.

Tab. S10 Calculated electronic transition data in terms of excitation energies (E/eV), emission wavelengths (λ_{em}/nm), oscillator strengths (f_{em}), and electronic compositions for **[DCF-MPYA-2H]$^{2-}$** and **[FL-2H]$^{2-}$** in DMSO.

Compound	Electronic transition[a]	Excitation energy (λ_{ab}/nm)	f [b]	Composition [c]	CI [d]
[DCF-MPYA-2H]$^{2-}$	$S_1 \rightarrow S_0$	2.17 eV (571)	0.335	H→L	0.64
	$S_2 \rightarrow S_0$	2.44 eV (508)	0.498	H→L+1	-0.58
[FL-2H]$^{2-}$	$S_1 \rightarrow S_0$	2.12 eV (586)	0.306	H→L	0.68
	$S_2 \rightarrow S_0$	2.40 eV (517)	1.024	H→L+1	0.69

[a] Only selected excitation states were considered. The numbers in parentheses are the excitation energy in wavelength. [b] Oscillator strength. [c] H stands for HOMO and L stands for LUMO. Only the configurations are presented. [d] Coefficient of the wave function for excitations. The CI coefficients are in absolute values.
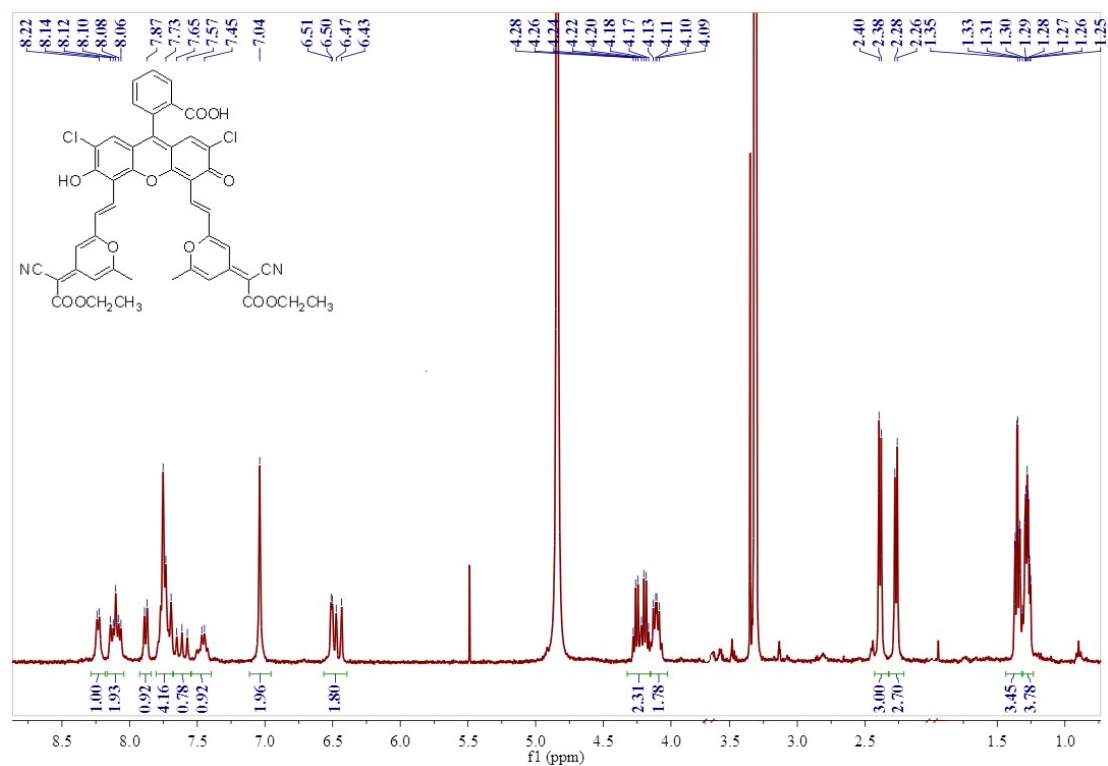
Fig. S21 ^{1}H-NMR spectrum of compound **DCF-MPYA**
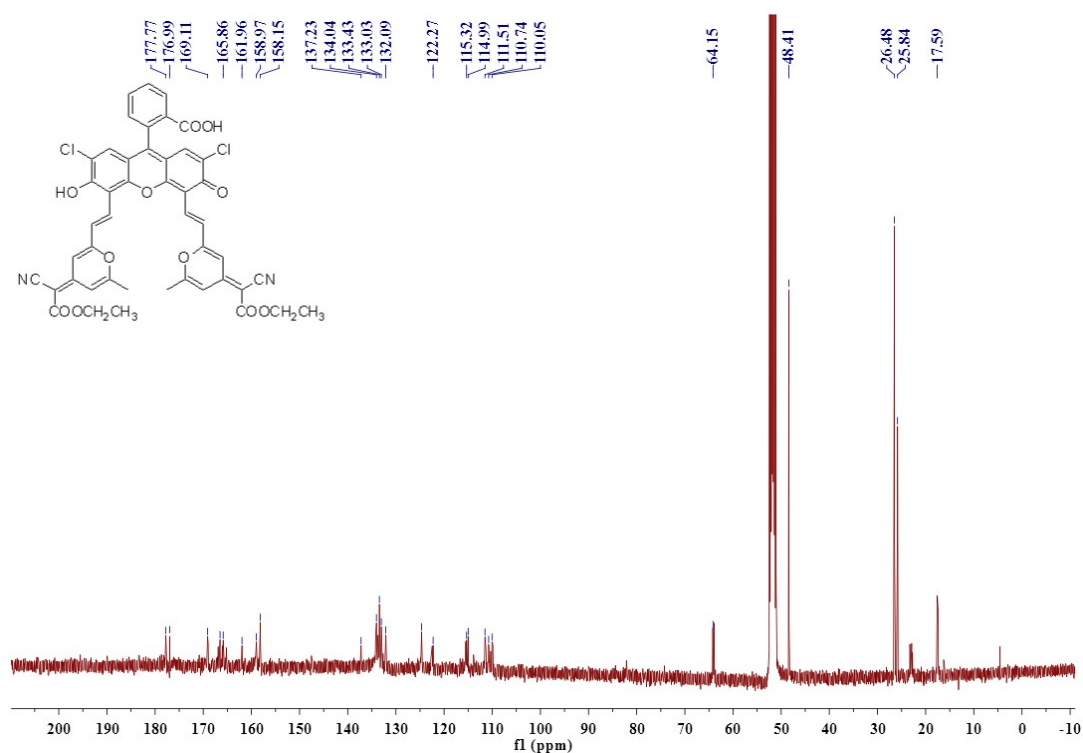
Fig. S22 ^{13}C spectrum of compound **DCF-MPYA**
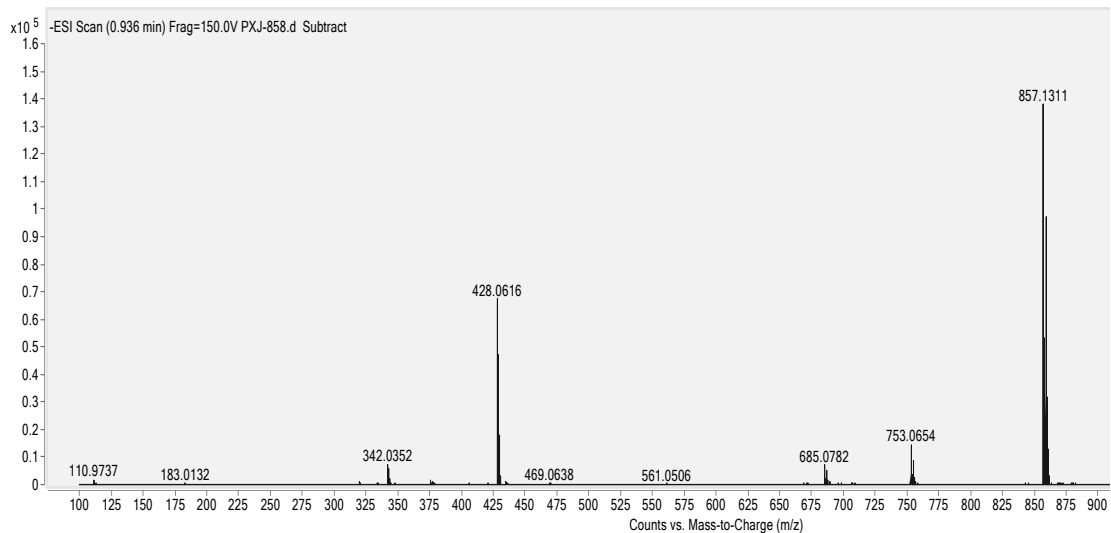
Fig. S23 HRMS spectrum of compound **DCF-MPYA**
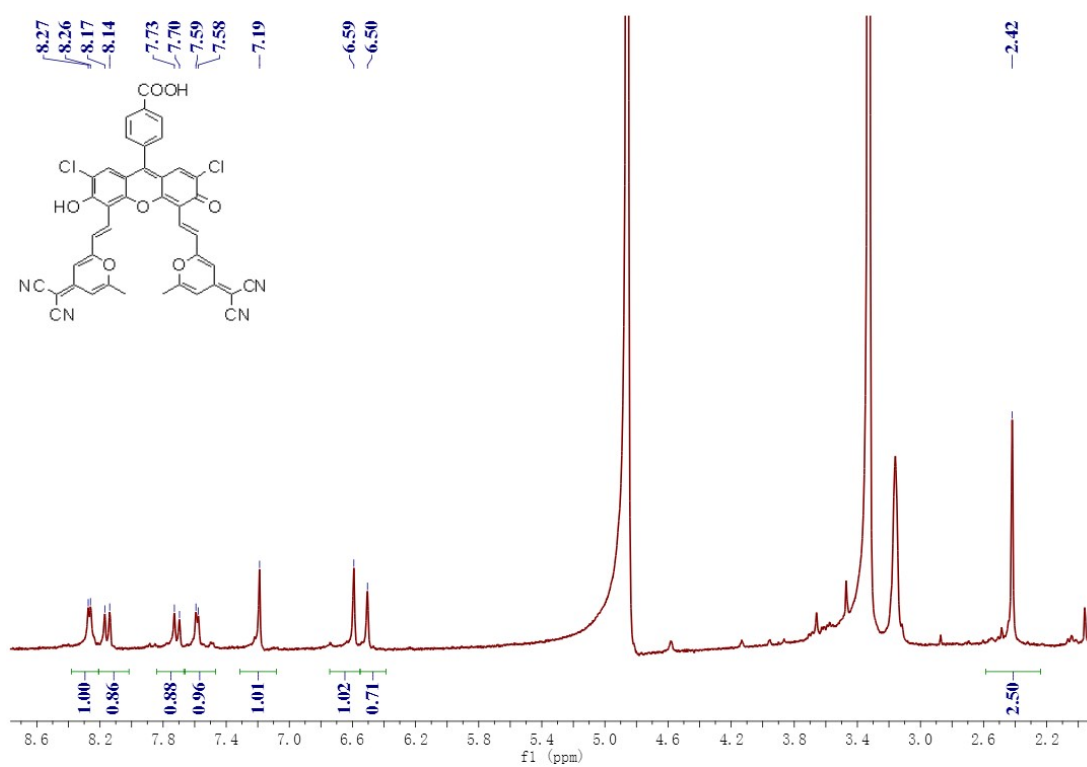
Fig. S24 ^{1}H-NMR spectrum of compound **FL**
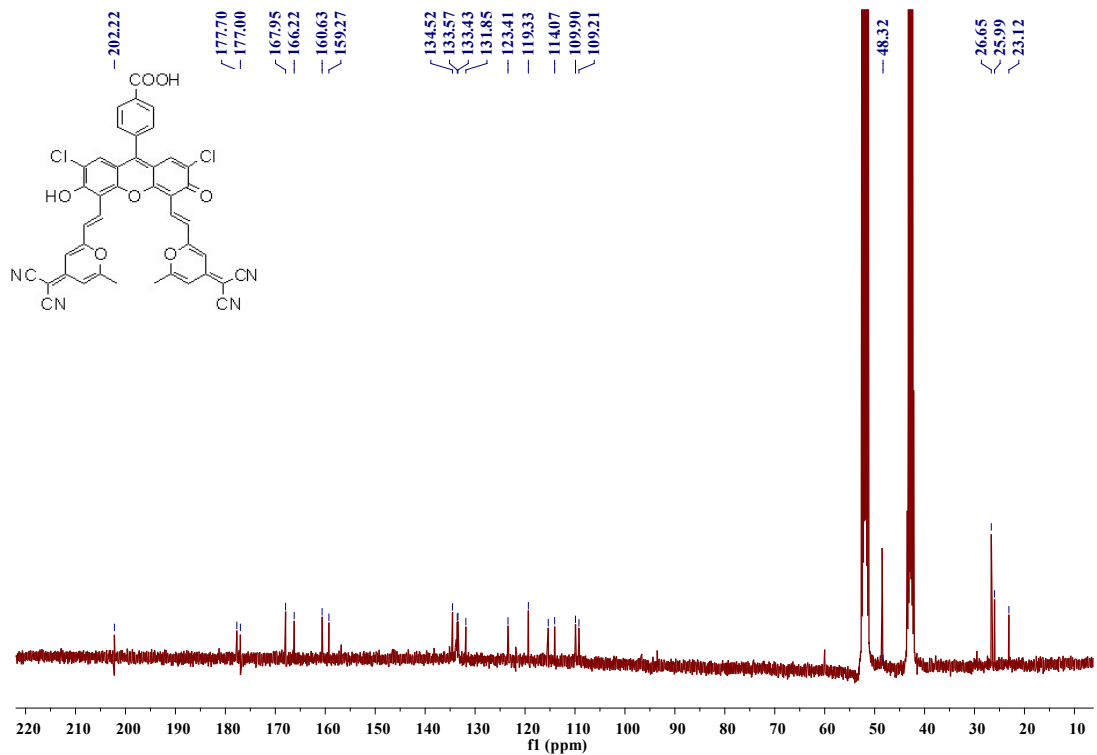
Fig. S25 ^{13}C spectrum of compound **FL**
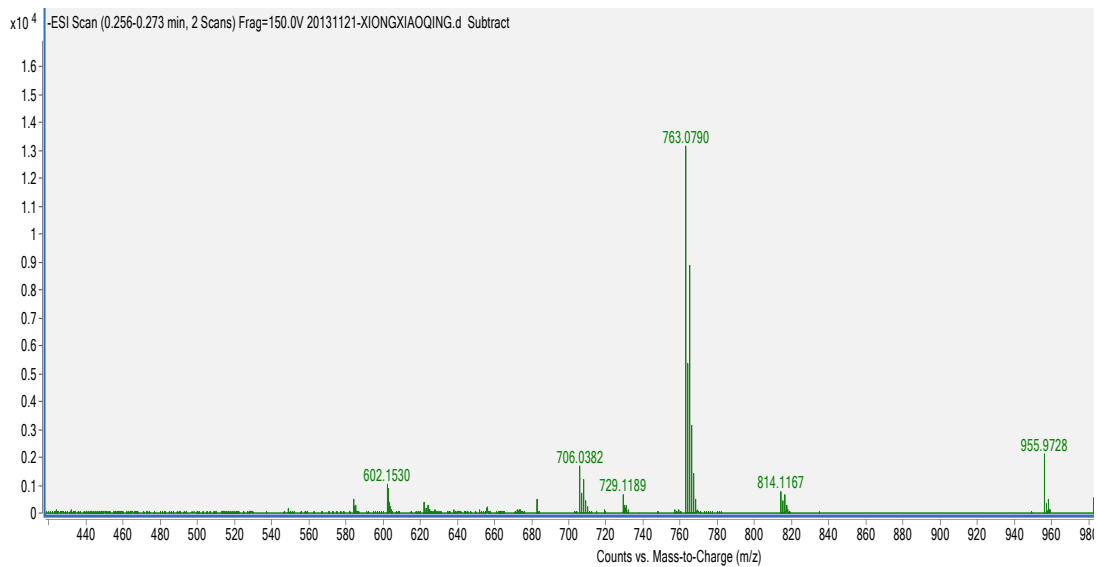
Fig. S26 HRMS spectrum of compound **FL**

References

[1] Grimme, S.; Bannwarth, C.; Dohm, S.; Hansen, A.; Pisarek, J.; Pracht, P.; Seibert, J.; Neese, F. Fully Automated Quantum-Chemistry-Based Computation of Spin-Spin Coupled Nuclear Magnetic Resonance Spectra. Angew. Chem., Int. Ed., 2017, 56, 14763−14769.

[2] Bannwarth, C.; Ehlert, S.; Grimme, S. Gfn2-Xtb-an Accurate and Broadly Parametrized Self-Consistent Tight-Binding Quantum Chemical Method with Multipole Electrostatics and Density-Dependent Dispersion Contributions. J. Chem. Theory Comput., 2019, 15, 1652−1671.

[3] Xtb, Version 6.1; University Bonn: 2019; please contact xtb@thch.uni-bonn.de for access to the program.

[4] Grimme, S. Exploration of Chemical Compound, Conformer, and Reaction Space with Meta- Dynamics Simulations Based on Tight-Binding Quantum Chemical Calculations. J. Chem. Theory Comput., 2019, 15, 2847−2862.

[5] Frisch, M. J.; Trucks, G. W.; Schlegel, H. B.; Scuseria, G. E.; Robb, M. A.; Cheeseman, J. R.; Scalmani, G.; Barone, V.; Mennucci, B.; Petersson, G. A.; Nakatsuji, H.; Caricato, M.; Li, X.; Hratchian, H. P.; Izmaylov, A. F.; Bloino, J.; Zheng, G.; Sonnenberg, J. L.; Hada, M.; Ehara, M.; Toyota, K.; Fukuda, R.; Hasegawa, J.; Ishida, M.; Nakajima, T.; Honda, Y.; Kitao, O.; Nakai, H.; Vreven, T.; Montgomery, J. A., Jr; Peralta, J. E.; Ogliaro, F.; Bearpark, M.; Heyd, J. J.; Brothers, E.; Kudin, K. N.; Staroverov, V. N.; Kobayashi, R.; Normand, J.; Raghavachari, K.; Rendell, A.; Burant, J. C.; Iyengar, S. S.; Tomasi, J.; Cossi, M.; Rega, N.; Millam, J.

M.; Klene, M.; Knox, J. E.; Cross, J. B.; Bakken, V.; Adamo, C.; Jaramillo, J.; Gomperts, R.; Stratmann, R. E.; Yazyev, O.; Austin, A. J.; Cammi, R.; Pomelli, C.; Ochterski, J. W.; Martin, R. L.; Morokuma, K.; Zakrzewski, V. G.; Voth, G. A.; Salvador, P.; Dannenberg, J. J.; Dapprich, S.; Daniels, A. D.; Farkas, O.; Foresman, J. B.; Ortiz, J. V.; Cioslowski, J.; Fox, D. J. Gaussian 09, Revision A. 02.

[6] Adamo, C.; Barone, V. Toward reliable density functional methods without adjustable parameters: The PBE0 model. J. Chem. Phys., 1999, 110, 6158−6170.

[7] Grimme, S.; Ehrlich, S.; Goerigk, L. Effect of the damping function in dispersion corrected density functional theory. J. Comput. Chem., 2011, 32, 1456−1465.

[8] Luchini, G.; Alegre-Requena, J. V.; Funes-Ardoiz, I.; Paton, R. S. GoodVibes: Automated Thermochemistry for Heterogeneous Computational Chemistry Data. F1000Res. 2020, 9, 291.

[9] (a) Grimme, S. Supramolecular Binding Thermodynamics by Dispersion-Corrected Density Functional Theory. Chem.−Eur. J., 2012, 18, 9955−9964. (b) Li, Y.-P.; Gomes, J.; Sharada, S. M.; Bell, A. T.; Head-Gordon, M. Improved Force-Field Parameters for QM/MM Simulations of the Energies of Adsorption for Molecules in Zeolites and a Free Rotor Correction to the Rigid Rotor Harmonic Oscillator Model for Adsorption Enthalpies. J. Phys. Chem. C, 2015, 119, 1840−1850.

[10] (a) B. Mennucci and J. Tomasi, Continuum Solvation Models: A New Approach to the Problem of Solute's Charge Distribution and Cavity Boundaries, J. Chem. Phys., 1997, 106, 5151–5158; (b) V. Barone and M. Cossi, Quantum Calculation of

Molecular Energies and Energy Gradients in Solution by a Conductor Solvent Model,

J. Phys. Chem. A, 1998, 102, 1995–2001.

[11] Legault, C. Y. CYLView, version 1.0b; Université de Sherbrooke: Sherbrooke, Quebec, Canada, 2009.

[12] Michael W. Allen, Thermo Fisher Scientific, Madison, WI, USA 2010.